## Supplemental Material

## Expanded Methods

*Generation, characterization and use of αMHC-miR-133a and αMHC-miR-378 transgenic mice.* Transgenic mice were created via cloning of a genomic DNA fragment flanking the mmu-miR-133a-1 or mmu-miR-378a microRNA stem-loop precursor regions into the SalI/HindIII cloning site of the αMHC/*Myh6* cardiac transgenic promoter construct [1], as previously described [2, 3]. Male mice between the ages of 8-12 weeks were used for these studies. Pressure-overload hypertrophy was induced via transverse aortic constriction (TAC) performed at Washington University's Mouse Cardiovascular Phenotyping Core (Dr. Carla Weinheimer, director). For miR-133a studies, 3 nontransgenic littermate controls and 7 αMHC-miR-133a mice were subjected to sham surgery; 5 nontransgenic and 4 αMHC-miR-133a mice were subjected to TAC. For miR-378 studies, 3 nontransgenic littermate controls and 3 αMHC-miR-378 mice were subjected to sham surgery while 7 mice of each genotype were subjected to TAC. Mice were housed and surgeries were performed according to procedures approved by the Washington University Animal Studies Committee.

*Tissue harvest and RNA preparation.* Hearts were placed in ice-cold saline, rinsed, and sectioned into 5-6 coronal slices. One was immediately fixed in 10% neutral buffered formalin for later histological analysis, while right ventricle fragments were removed from the others prior to flash-freezing in liquid nitrogen. Total RNA was prepared from flash-frozen sections (or from saline-rinsed cell monolayers; see below) using Trizol (Invitrogen) as per the manufacturer's directions, with the exception that isopropanol precipitation was carried out for 30 min at room temperature to improve small RNA yield. Ago2 immunoprecipitation prior to RNA isolation for RISC-sequencing was carried out as detailed below.

*Mouse adult cardiomyocyte isolation and gene expression analysis.* Cardiomyocyte and fibroblast fractions were separately isolated from the hearts of three 8 week-old, wild-type FVB/N mice, as previously described [4]. Following 3 rounds of gravity filtration and washing with ice-cold PBS, myocytes were immediately dissolved in Trizol (Invitrogen) and total RNA was prepared. In order for sufficient nonmyocytes (fibroblasts) to be available for gene expression assays, cells were plated in tissue culture dishes in DMEM / 10% fetal calf serum / antibiotics, grown at 37°C / 5% $CO_2$, and passaged once. Cell monolayers were harvested directly into Trizol. Previously, Applied Biosystems TaqMan microRNA and mRNA qPCR assays were performed on these total RNA preparations [3]. All samples were subsequently assayed by microRNA-sequencing and mRNA-sequencing (described below), and both raw sequencing data and per-gene tabulated data have been deposited in NCBI GEO GSE58453. We defined a 'cardiomyocyte enrichment ratio' as [0.6*(FPKM in myocytes)]/[0.4*(FPKM in nonmyocytes)] to model the approximate 60%:40% ratio of cardiomyocyte to nonmyocyte mass [5]. Cardiomyocyte-enriched mRNAs were selected at an enrichment ratio ≥2, nonmyocyte-enriched mRNAs were selecte at an enrichment ratio ≤0.5, and those with intermediate values were defined as nonenriched for either cell fraction. For a small number of mRNAs, detection was not possible in isolated cardiomyocyte or nonmyocyte fractions; these are classified as 'unknown enrichment' in data tables.

*microRNA annotation using miRBase 21.* Previous nomenclature for microRNAs often described the minor product (passenger strand) of a microRNA stem-loop structure as a miR* form. In this manuscript, we have annotated mouse microRNAs according to the nomenclature used by miRBase 21, released in June 2014 (http://www.mirbase.org/) [6, 7]. microRNAs are designated as -5p or -3p forms according to their site of origin in the microRNA stem-loop precursor. While information on whether a microRNA form is 'major' or 'minor' is sometimes available from deep-sequencing data accumulated in the miRBase database from a variety of tissues, we designate 'major' and 'minor' forms in mouse hearts according to previously obtained deep-sequencing data [3]. For convenience, 'miR-133a' refers to mmu-miR-133a-3p and 'miR-378' refers to mmu-miR-378a-3p unless otherwise mentioned.

*microRNA-Seq for microRNA expression analysis.* Libraries were prepared with TruSeq Small RNA Sample Prep Kits (Illumina) following the manufacturer's protocols, as previously described [8]. Briefly, small RNAs from 1 μg total cardiac RNA were sequentially ligated with 3′ and 5′ adapters, followed by reverse transcription to produce single stranded cDNAs, which were then amplified by PCR with primers including indexing capabilities to distinguish individual libraries after flowcell processing. The amplified libraries were size-selected/gel-purified and quantified. Twelve libraries were pooled in equimolar amounts and diluted to 14 pmol/L for cluster formation on a single flow cell lane, followed by single-end sequencing (50 nt reads, not including the index determination) on an Illumina HiSeq 2000 sequencer. Alignment and quantitation of microRNA sequencing reads was performed using sRNAbench (http://bioinfo5.ugr.es/sRNAbench/sRNAbench.php)[9].

*mRNA-Seq for mRNA expression analysis.* mRNA-sequencing was performed essentially as described [8, 10-12], using Illumina HiSeq 2000 sequencers and library indexing. Using prior criteria that a meaningfully expressed transcript should be present at a level equivalent to at least 1 mRNA copy/cell (3 FPKM; fragment [reads] per kilobase of exon per million mapped reads) [8, 10-12], or as an alternate, that a detectable transcript must map to at least 1 millionth of the total mapped reads in an individual library, we identified approximately 13,000 coding mRNAs in mouse hearts. Concordance of these cardiac transcriptomes with those from previous RNA-Seq studies was high [8, 10-12].

We and others have extensively compared RNA-sequencing analyses to microRNA and mRNA microarrays, finding that RNA-sequencing analyses generally offer superior dynamic range and accuracy (Supporting Information of [8]). In addition, we have validated differential expression results from sequencing analyses with RT-qPCR techniques in several prior studies [8, 10, 13].

*RISC-Seq for microRNA-dependent mRNA expression analysis.* Ago2 was immunoprecipitated from coronal sections of the same hearts used for mRNA-sequencing, followed by total RNA isolation from the Ago2 immunoprecipitate, as described in [10] and the Supplemental Material of [8].

*Alignment and quantitation of mRNA-Seq and RISC-Seq reads.* Single-end, 50 nt reads were obtained from Illumina HiSeq 2000 sequencers. Following separation of libraries according to 3' indexes, both mRNA-Seq and RISC-Seq reads were aligned against the mouse transcriptome genes.gtf file defined from UCSC mm10 and present in the Illumina iGenomes package April 2014, using Tophat 2.0.10 (http://ccb.jhu.edu/software/tophat/index.shtml) [14, 15] to generate bam files and HTSeq (http://www-huber.embl.de/users/anders/HTSeq/doc/overview.html) to allocate

reads to gene locations. Tophat version 2 allows preparation of a pre-defined transcriptome (i.e. according to those genes defined in the genes.gtf list) to which reads are mapped; since ribosomal RNAs are not present in this list and these represent the major non-mRNA type in Ago2 immunoprecipitates, this allows for read mapping only to defined mRNAs in both RISC and global mRNA fractions. HTSeq read data were used as input for statistical calculations, including fold-change and false discovery rate determination, by the DESeq package [16] (see below). Cufflinks (version 2) (http://cufflinks.cbcb.umd.edu/) [14] was used to obtain FPKM values from bam files for presentation and inter-study comparison purposes,

For mRNA-seq, mean raw reads per heart were $(2.08 \pm 0.11) * 10^7$, mean alignment to the transcriptome was $(61.4 \pm 0.8)$%, and mean aligned reads per heart were $(1.26 \pm 0.06) * 10^7$.

For RISC-seq, mean raw reads per heart were $(2.67 \pm 0.19) * 10^7$, mean alignment to the transcriptome was $(31.5 \pm 1.4)$% (since a greater proportion of the raw reads comprised non-mRNA), and mean aligned reads per heart were $(0.77 \pm 0.04) * 10^7$.

Detectable mRNAs were defined as those with at least 6 aligned reads (~1 millionth of the read depth of the lower RISC-seq libraries) in at least 50% of the samples. A total of 13,328 mRNAs were analyzed in downstream procedures.

All mRNA-Seq and RISC-Seq data from this study have been deposited in the NCBI GEO under accession GSE65141 (miR-133a cohort) and GSE61734 (miR-378 cohort). Relative abundance of microRNAs in intact hearts are under accession GSE55791, while microRNA abundances in cardiomyocyte and fibroblast fractions are under accession GSE58453.

*Calculation of differential gene expression using the DESeq package.* DESeq [16] (version 1) was used to normalize read depth across multiple sequencing libraries, to calculate fold-changes, and to derive individual pairwise comparison p-values and false discovery rates (FDRs). While DESeq takes the non-normalized, absolute number of aligned reads as input, we reported RISC RNA and global mRNA abundance as FPKM, although the underlying fold-change and p-value / FDR comparisons used DESeq's internal methods of library normalization. DESeq is part of the Bioconductor open-source software suite for the R statistical environment (http://bioconductor.org/packages/release/bioc/html/DESeq.html).

*Differential expression cutoff thresholds and other statistics.* Unless otherwise defined, regulated RNAs were defined using a threshold of 25% (increased or decreased) at an FDR of 0.02. Partek Genomics Suite 6.6 (Partek, St. Louis, MO) was used to derive principal components analysis plots and unsupervised hierarchical clustering heatmaps. Unpaired, 2-tailed t-tests (for parametric data) or Mann-Whitney U tests (for nonparametric data), or ANOVA tests were used for comparison of physiological parameters between mice and significance was taken at $P<0.05$. Assessment of parametric distribution prior to ANOVA was made with a D'Agostino-Pearson omnibus normality test, and Bartlett's test was used to assess homoscedasticity (GraphPad Prism 6 software).

*Classification of individual mRNAs according to dependence of regulation on microRNAs*

Considering numerous recent studies demonstrating translational suppression without detectable mRNA transcript degradation [17-21] we have widened the scope of our RISC analyses here, in

comparison to previous studies [8, 10, 11], to classify regulated mRNAs into one of several possible categories of microRNA dependency. These are:

1) reciprocal regulation in RISC and global mRNA fractions, as used in prior studies [8, 10];

2) regulation only in the RISC fraction, implying an effect on translation without altering transcript levels;

3) regulation only at the global mRNA level, showing lack of direct targeting by microRNAs; and

Direct microRNA targets (microRNA-dependent mRNAs) are obtained from categories 1 and 2, while indirect targets (microRNA-independent mRNAs) are obtained from category 3.

*Informatic suites.* MetaCore [22] (http://thomsonreuters.com/metacore) was used for pathway map and process network classification, while DAVID [23] was used for Gene Ontology annotation.

*RT-qPCR assays*. TaqMan RT-qPCR assays for microRNAs and mRNAs were performed as previously described [8] using the following probes:

TaqMan miR-133a-3p: mmu-miR-133a, #002246
TaqMan miR-378a-3p: mmu-miR-378, #002243
TaqMan U6 snRNA: RNU6, #001973

For quantitation of pre-miRs, oligo(dT) was used to reverse transcribe 1 μg of total RNA using SuperScript III (Invitrogen) and 5% of the resulting product was used as input in qPCR with SybrGreenER supermix (Invitrogen). Primers for pre-miR-133a were: forward 5'-GAGCTGGTAAAATGGAACCAAA-3', reverse 5'- ACAGCTGGTTGAAGGGGAC-3', 61 bp product. Primers for pre-miR-378 were: forward 5'- AGGGCTCCTGACTCCAGGT-3', reverse 5'-GTGACTCCACTCAGGCCTTCT-3', 78 bp product. Reference RNAs to normalize pre-miR data were Gapdh (TaqMan Mm99999915_g1) and Actb (TaqMan Mm01205647_g1).

*Fluorescent lectin staining, cross-sectional area and length determinations*. Formalin-fixed, paraffin-embedded cardiac tissue was sectioned at 4 μm onto coated glass slides. Following deparaffinization in mixed xylenes, graded ethanol washes and three 5 min washes in phosphate-buffered saline (PBS), slides were incubated with 100 μg/mL Alexa Fluor 488-coupled wheat germ agglutinin (Molecular Probes) in PBS containing 1 mM $CaCl_2$ for 60 min, room temperature, in dark conditions. Following 3 further washes in PBS, slides were mounted in VectaShield + DAPI (Vector Laboratories) and imaged for AF488 and DAPI fluorescence.

The area enclosed by AF488-fluorescent borders was obtained from an average of 500 non-elongated (rounded) cells per heart, with identifiable nuclei, and defined as myocyte cross-sectional area. Similarly, tissue sectioned in parallel to the long axis of myocytes was used to determine myocyte length, using elongated cells with recognizable nuclei and with clearly defined borders to demarcate their long axes. An average of 100 cells per heart with sharp border definition were used for length measurements.

*Immunoblot analysis of cardiac proteins.* Proteins from cardiac homogenates (prepared in the presence of protease inhibitors) were separated using 10% SDS-PAGE and transferred to

Immobilon-FL low-fluorescence PVDF membranes (Millipore). Heart sections were homogenized in ice-cold 50 mmol/L Tris, 5 mmol/L EDTA and 5 mmol/L EGTA, pH 7.6, containing Complete protease inhibitors (Roche), and all subsequent procedures were performed at 4 C. Debris was removed at 200*g*, 5 min, followed by nuclear removal at 1000*g*, 10 min. NP-40 (Sigma IGEPAL CA-630) was added at 0.2% (vol/vol) to the supernatant. After 15 min rocking, insoluble material was removed at 10000*g*, 10 min. A Bradford stain-based colorimetric dye assay (Bio-Rad) was used to determine protein concentration. For GAPDH and alpha-tubulin detection, 10 μg of NP-40-solubilized cardiac protein was separated on precast 4-20% SDS-PAGE minigels (Bio-Rad). Electrophoretic transfer to PVDF was achieved in 25 mmol/L Tris, 192 mmol/L glycine and 20% (vol/vol) methanol.

Primary antibody against Ago2 was the same used for immunoprecipitation; Wako Pure mouse monoclonal anti-Ago2 (at 0.5 μg/mL), catalog #018-222021, clone 2D4. Primary antibody against GAPDH was Abcam #8245 mouse anti-GAPDH, 1:5000, and primary antibody against alpha-tubulin was Sigma T6704 mouse anti-alpha-tubulin, 1:10000. All primary antibodies were diluted in LiCor Odyssey Blocking Buffer with 0.1% (vol/vol) Tween-20 and incubated with membranes overnight at 4 C. Bound primary antibodies were detected with LiCor IrDye-coupled goat anti-mouse (680LT) at 1:20000 in Odyssey Blocking Buffer with 0.1% (vol/vol) Tween-20 and 0.01% SDS. Signals were visualized and quantitated with a LiCor Odyssey digital imaging system and associated software [24].

*In vitro luciferase reporter assays for miR-378-mRNA interactions.* pCMV-MIR and pCMV-MIR-378 microRNA expression constructs were from OriGene Technologies (Rockville, MD); catalog numbers PCMVMIR and SC401025, respectively. HEK293T cells were transiently transfected in 96-well plates (6 replicates per transfection condition) with 180 ng pCMV-MIR construct and 30 ng luciferase reporter construct together with 1.2 μL Fugene HD per well, and both firefly and Renilla luciferase activity were measured after 48 h using the Dual-GLO Luciferase Assay reagents (Promega) as per the manufacturer's directions. The 3xGrb2 construct in pmiRGLO (Promega), containing 3 repeats of a Grb2-derived miR-378-binding sequence [25] was a kind gift from Madhu Gupta, University of Illinois, Chicago. The mouse Rapgef4 cDNA region was PCR-amplified and cloned into psiCheck2 (Promega) between XhoI and NotI sites (italicized) using the following primers: forward 5'-agccta*CTCGAG*acatctgaagtgcccagagt-3', reverse 5'-atgtat*GCGGCCGC*tatttcttgtcaagtatattta-3'.

**Additional Figures**

**Supplemental Figure 1**

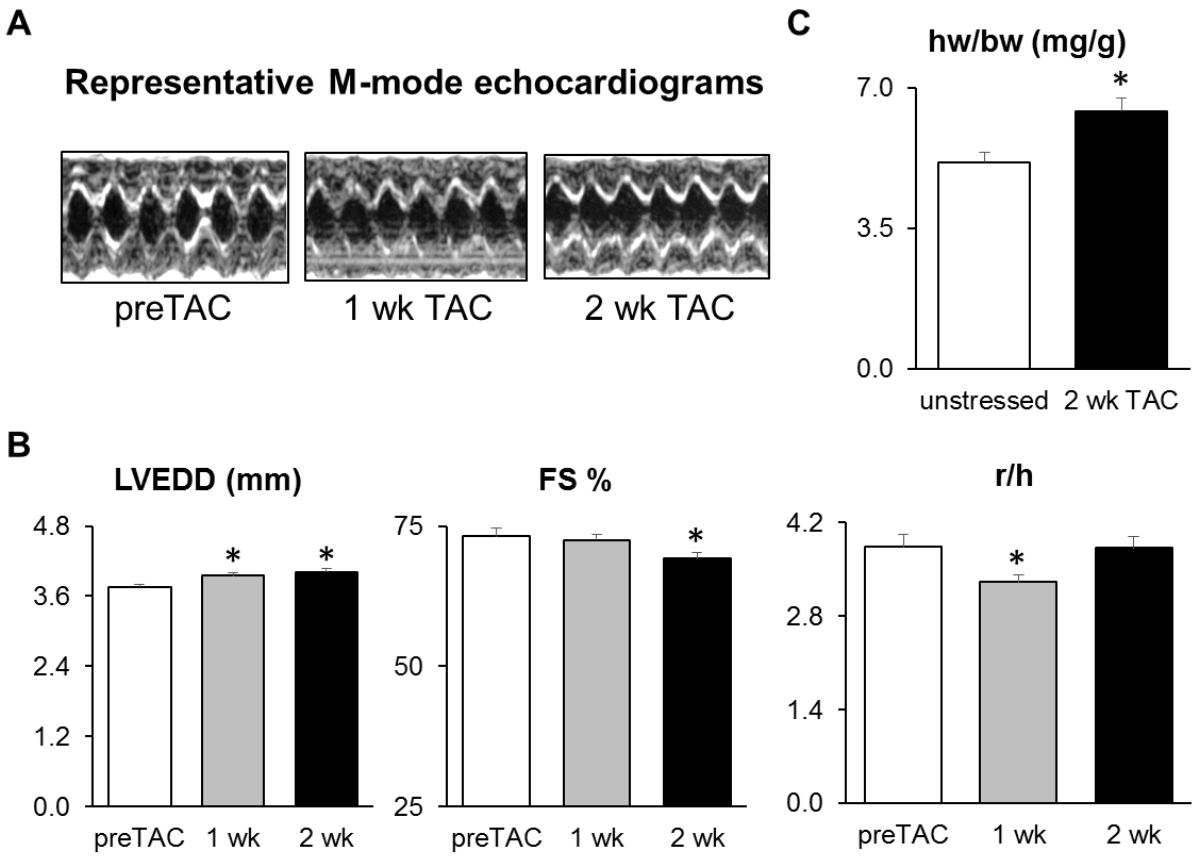


**Supplemental Figure 1.** Echocardiographic assessment of TAC progression. **A**) Representative M-mode echocardiograms taken prior to and after TAC. **B**) Calculated echocardiographic parameters. **C**) Gravimetric heart weight relative to body weight. FVB/N nontransgenic mice, n=4-6 per group, mean ± s.e.m. * $p<0.05$ relative to preTAC or unstressed, unpaired t-test.

**Supplemental Figure 2**

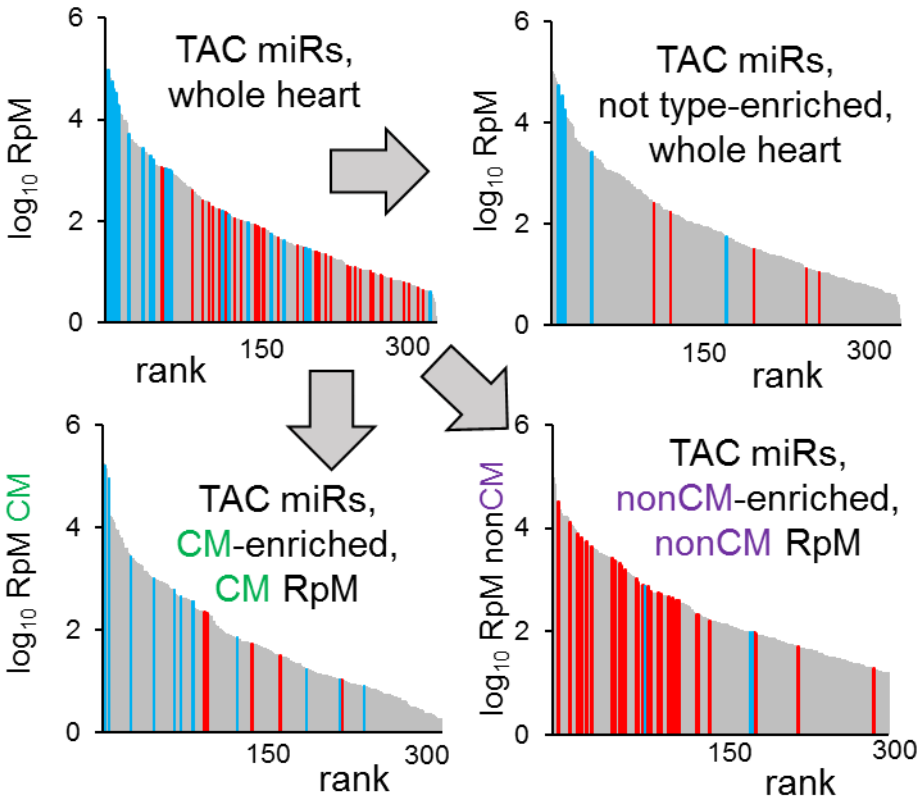


**Supplemental Figure 2.** Cardiomyocyte and nonmyocyte distribution of microRNAs regulated after 1 wk TAC. Cardiomyocytes and nonmyocytes were obtained from FVB/N nontransgenic hearts and subjected to small RNA-sequencing; this procedure and the definition of enrichment by cell type are described in **Expanded Methods.** RpM, reads per million reads mapped to microRNAs. Red bars, microRNAs upregulated in TAC vs sham whole-heart RNA preparations, FDR<0.02; blue bars, downregulated microRNAs.

**Supplemental Figure 3**

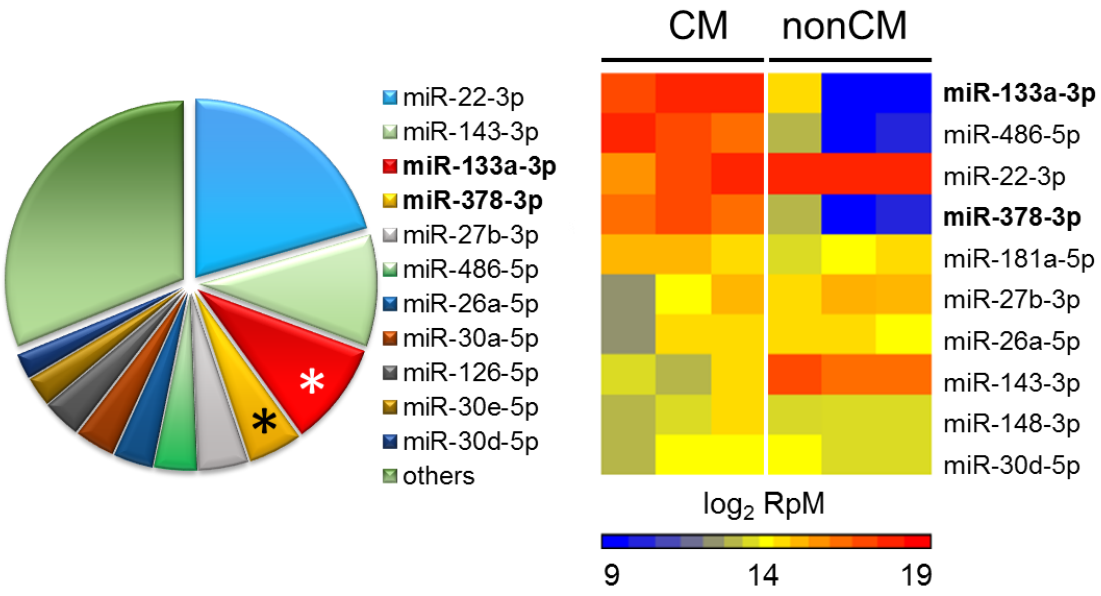


**Supplemental Figure 3.** Cardiomyocyte and nonmyocyte distribution of abundant cardiac microRNAs. MicroRNA abundances defined by miR-sequencing of intact adult FVB/N mouse hearts (pie chart) and of isolated cardiomyocytes and nonmyocytes / fibroblasts (heatmap). RpM, reads per million reads mapped to microRNAs.

**Supplemental Figure 4**

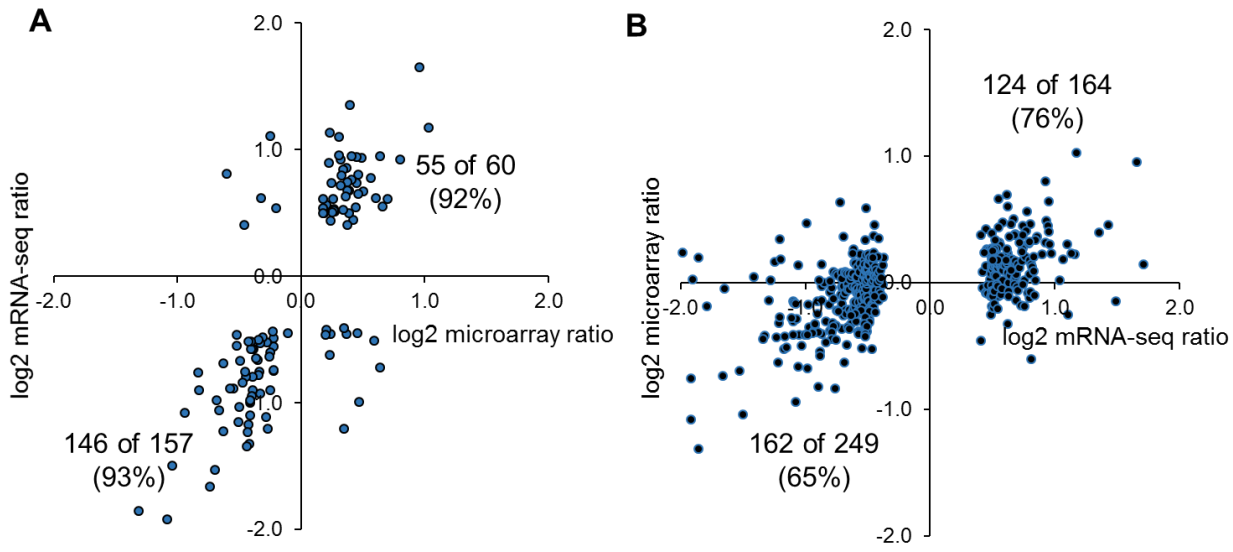


**Supplemental Figure 4.** Similarity of mRNA-sequencing and microarray data for αMHC-miR-133a-affected mRNA transcripts. **A**, 217 significantly regulated ($p<0.05$) mRNAs from microarray (x-axis) [2] *vs* regulation obtained from RNA-sequencing in the present study (y-axis). As expected, RNA-sequencing reveals a wider dynamic range of mRNA regulation than that observed from microarray measurements [13]. **B**, 413 significantly regulated mRNAs from RNA-sequencing (fold-change 25%, FDR<0.02) (x-axis) plotted against regulation observed from microarrays [2]. Here, the more limited dynamic range of microarray determination tends to reduce the gradient of a linear correlation line.

**Supplemental Figure 5**

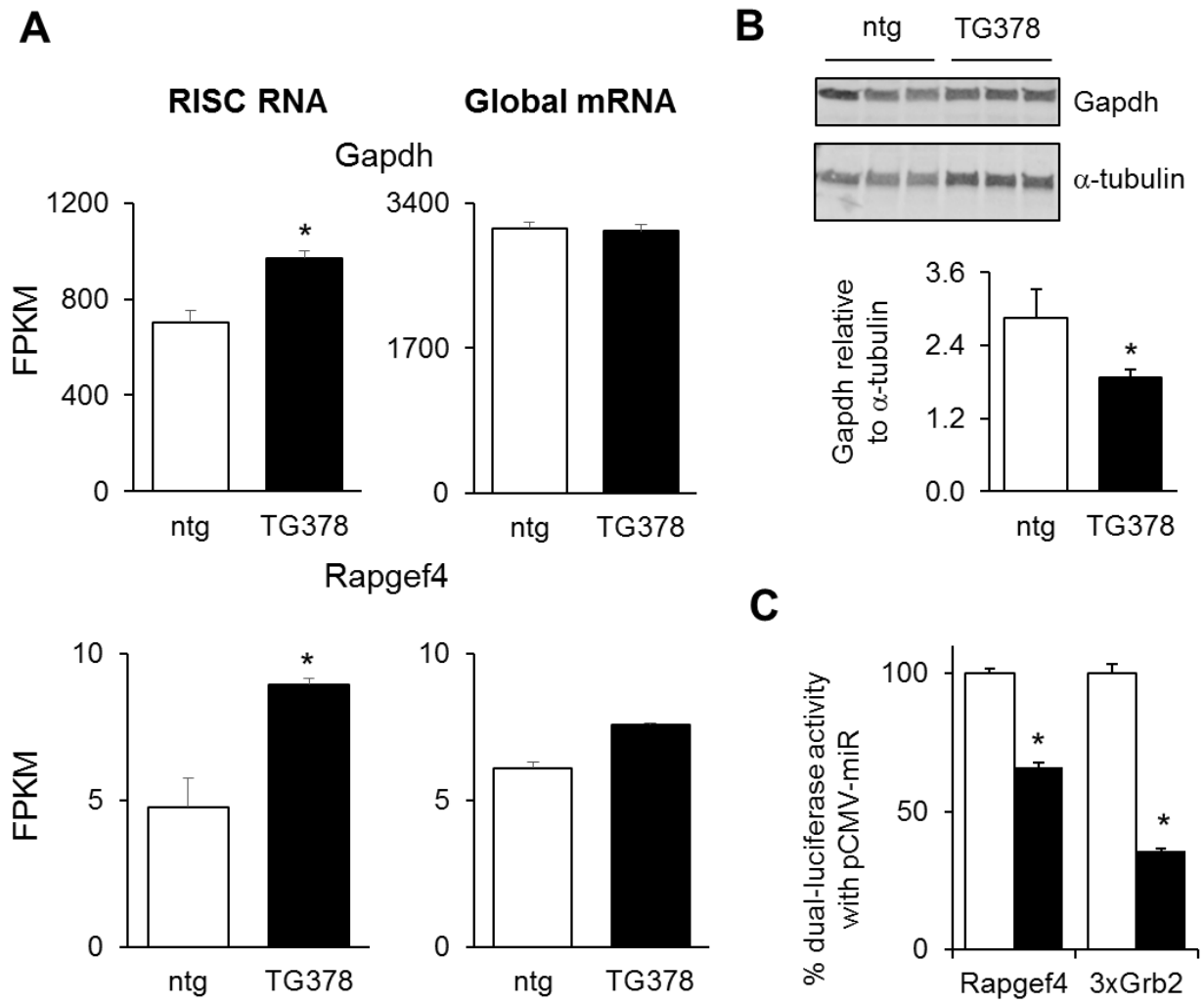


**Supplemental Figure 5.** Validation of translational suppression predicted from RISC-sequencing. **A**) Gapdh and Rapgef4 were two mRNAs predicted to be translationally suppressed from data indicating increased RISC abundance without global mRNA abundance changes in unstressed αMHC-miR-378 hearts. * FDR<0.02 compared to nontransgenic hearts. **B**) Immunoblot data demonstrating decreased Gapdh relative to aggregate alpha-tubulin (i.e. the protein products of *Tuba1a*, *Tuba1b*, *Tuba1c*, *Tuba4a* and *Tuba8*) in αMHC-miR-378 vs nontransgenic hearts (n=3 each; graph shows quantitative data, mean ± s.e.m., * p<0.05 relative to nontransgenic). **C**) miR-378-directed suppression (luciferase reporter assay) of a cloned fragment of Rapgef4 in HEK293T cells (**Expanded Methods**); comparison to a previously published 3xGrb2 construct [25] is shown. * p<0.05 relative to pCMVmiR (empty microRNA precursor plasmid vector) transfection, white bars; pCMVmiR-378, black bars.

**Supplemental Figure 6**

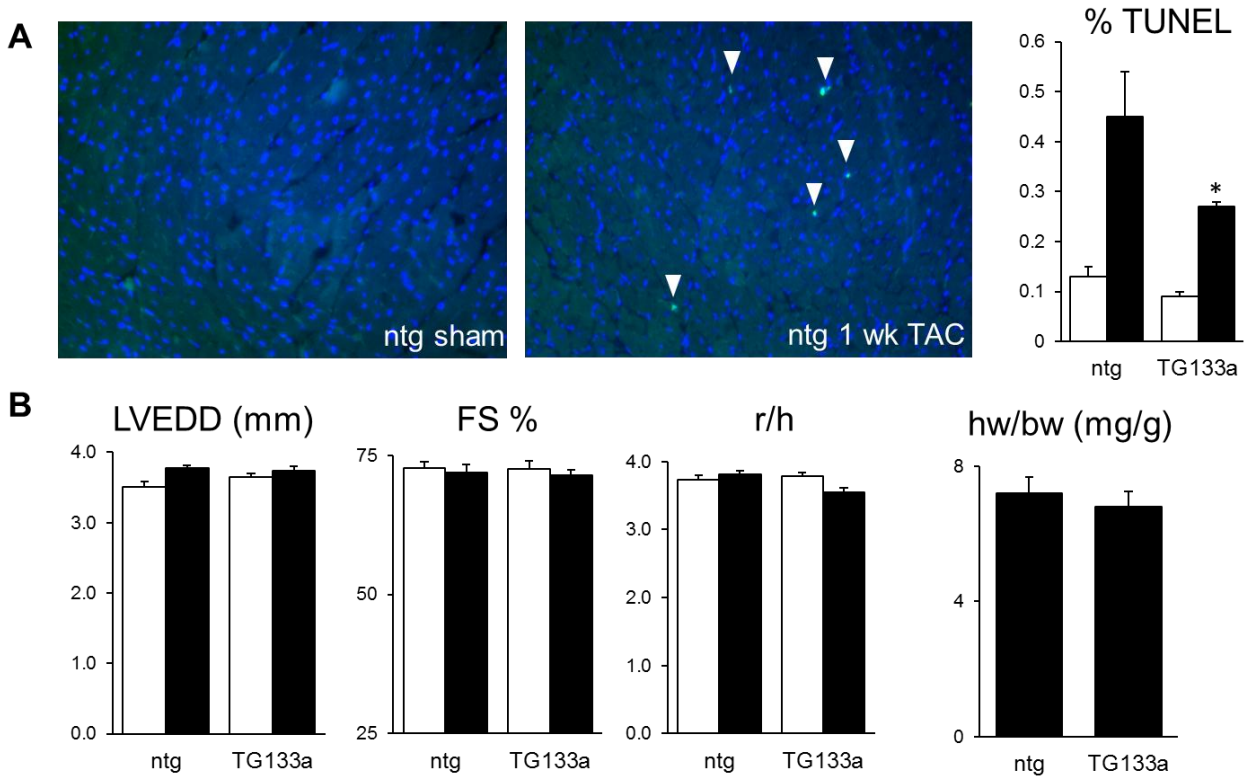


**Supplemental Figure 6.** Recapitulation of apoptosis and hypertrophy findings from αMHC-miR-133a mice after 1 wk. **A**) Reduced TUNEL-positive myocytes were observed in αMHC-miR-133a hearts compared to nontransgenic hearts after 1 wk TAC, as originally reported [2]. **B**) In similar fashion, echocardiographic parameters were neither worsened nor improved in αMHC-miR-133a hearts at this timepoint, and the extent of gross hypertrophy (measured as gravimetric heart weight) did not differ [2].

**Supplemental Figure 7**

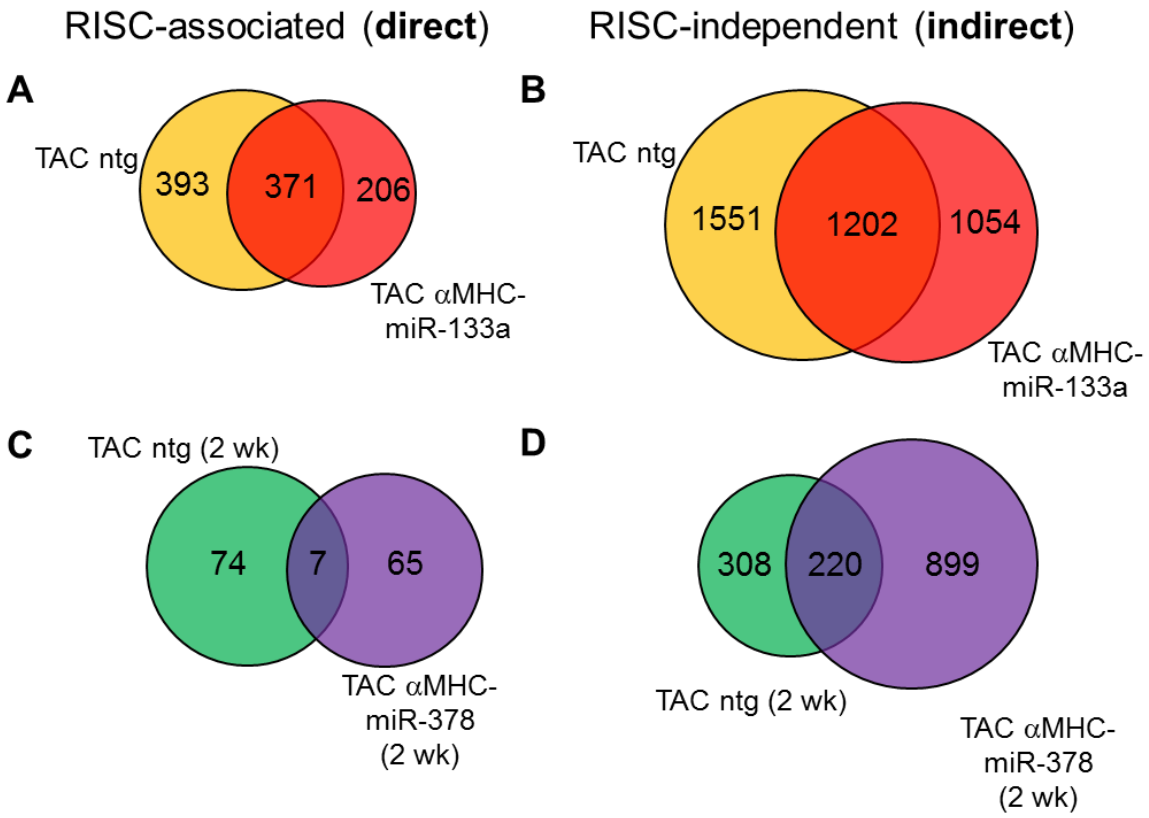


**Supplemental Figure 7.** MicroRNA transgene effects on TAC mRNA targets identified from RISC-sequencing. Venn analyses of direct (**A**) and indirect mRNA targets (**B**) of 1 wk TAC in nontransgenic hearts (orange circles), compared to mRNAs regulated in a RISC-dependent or RISC-independent manner in TAC αMHC-miR-133a hearts (red circles). **C-D**) As for **A-B)**, but in αMHC-miR-378 hearts and with green circles denoting targets of 2 wk TAC in nontransgenic hearts.

**Supplemental Figure 8**

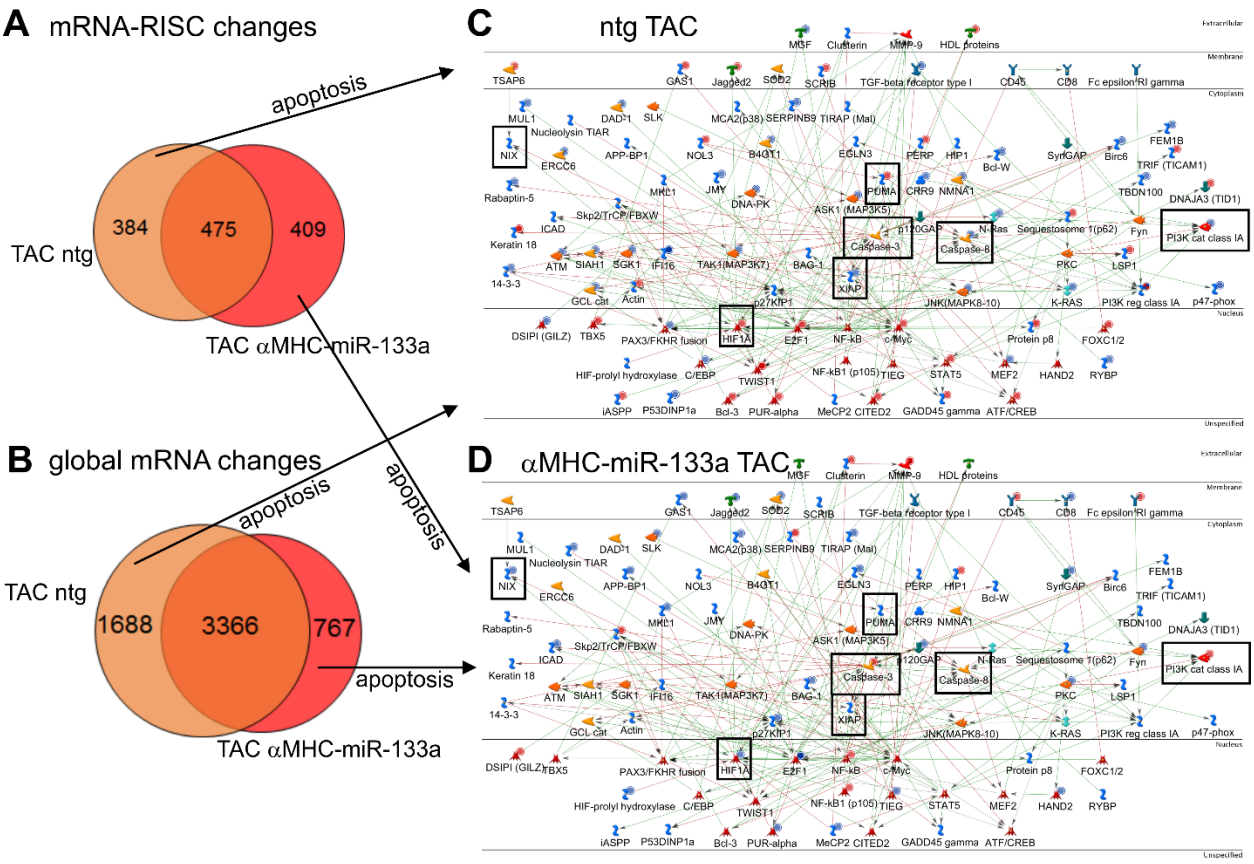


**Supplemental Figure 8.** Involvement of miR-133a-regulated mRNAs in apoptotic signaling pathways. Venn analyses of **A)** all RISC-dependent mRNA alterations and **B)** changes in global mRNA abundance during 1 week TAC in nontransgenic and αMHC-miR-133a hearts. All comparisons are relative to sham nontransgenic hearts. Genotype-unique 'apoptosis' genes in a MetaCore direct interaction network [22] with increased (marked with red dots) or decreased (marked with blue) translational potential are shown for **C)** nontransgenic TAC and **D)** αMHC-miR-133a TAC. Boxes designate particular mRNAs of interest.

**Additional Tables**

**Supplemental Table 1**

| Protein class | Actual | n | R | N | Expected | Ratio | p-value | z-score | In data set | In protein function | Protein function in database |
|---|---|---|---|---|---|---|---|---|---|---|---|
| **Transcription factors** | 24 | 383 | 883 | 21059 | 16.06 | 1.494 | 3.342E-02 | 2.043 | 6.27% | 2.72% | 4.19% |
| **Enzymes** | 58 | 383 | 2551 | 21059 | 46.4 | 1.25 | 4.274E-02 | 1.834 | 15.14 % | 2.27% | 12.11% |
| **Kinases** | 13 | 383 | 615 | 21059 | 11.19 | 1.162 | 3.295E-01 | 0.5559 | 3.39% | 2.11% | 2.92% |
| **Proteases** | 9 | 383 | 554 | 21059 | 10.08 | 0.8932 | 4.455E-01 | -0.3466 | 2.35% | 1.62% | 2.63% |
| **Receptors** | 22 | 383 | 1426 | 21059 | 25.93 | 0.8483 | 2.449E-01 | -0.8075 | 5.74% | 1.54% | 6.77% |
| **Phosphatases** | 2 | 383 | 211 | 21059 | 3.837 | 0.5212 | 2.588E-01 | -0.9514 | 0.52% | 0.95% | 1.00% |
| **Ligands** | 3 | 383 | 461 | 21059 | 8.384 | 0.3578 | 3.023E-02 | -1.897 | 0.78% | 0.65% | 2.19% |
| **Other** | 254 | 383 | 14409 | 21059 | 262.1 | 0.9693 | 2.004E-01 | -0.8938 | 66.32 % | 1.76% | 68.42% |

*Columns have the following meaning:*

**Protein class** a broadly defined protein function

**Actual** number of network objects from the activated dataset(s) for a given protein class

**n** number of network objects in the activated dataset(s)

**R** number of network objects of a given protein class in the complete database or background list

**N** total number of network objects in the complete database or background list

**Expected** mean value for hypergeometric distribution (n*R/N)

| | |
|---|---|
| **Ratio** | connectivity ratio (Actual/Expected) |
| **z-score** | z-score ((Actual-Expected)/sqrt(variance)) |
| **p-value** | probability to have the given value of Actual or higher (or lower for negative z-score) |
| **In data set** | fraction of network objects with a selected function in the activated dataset |
| **In protein function** | fraction of network with a selected function in the activated dataset among network objects with this function in the complete database or background list |
| **Protein function in database** | fraction of network objects with a selected function in the complete database or background list |

**Supplemental Table 1.** Functional categorization of mRNAs regulated by TAC in a microRNA-dependent manner. Direct and indirect mRNA targets (microRNA-dependent and –independent) identified using RISC-seq procedures were classified by MetaCore software [22] into protein functional groups. Although the definition of microRNA-dependent mRNAs was expanded compared to that previously used, the data recapitulate those of our earlier study [8].

**Supplemental Table 2.** microRNA-dependent mRNA regulation during 1 week of TAC in nontransgenic mice. Direct mRNA targets of microRNAs identified using RISC-seq procedures (**Expanded Methods**) are listed. Cardiomyocyte enrichment ratios for individual mRNAs are calculated as described in **Expanded Methods**. fc, fold-change; FDR, false-discovery rate; FPKM, fragments per kb of exon per million mapped (aligned) reads. Category designations are UN = RISC up, no global mRNA change; DN = RISC down, no global mRNA change; UD = RISC up, global mRNA down; DU = RISC down, global mRNA up.

**Supplemental Table 2** is supplied as an Excel (.xls) file.

**Supplemental Table 3.** microRNA-independent mRNA regulation during 1 week of TAC in nontransgenic mice. mRNAs not directly targeted by microRNAs identified using RISC-seq procedures (**Expanded Methods**) are listed. Cardiomyocyte enrichment ratios for individual mRNAs are calculated as described in **Expanded Methods**. fc, fold-change; FDR, false-discovery rate; FPKM, fragments per kb of exon per million mapped (aligned) reads. Category designations are NU = no RISC change, global RNA up; ND = no RISC change, global mRNA down.

**Supplemental Table 3** is supplied as an Excel (.xls) file.

**Supplemental Table 4.** Cardiomyocyte and nonmyocyte distribution of TAC-regulated mRNAs. mRNAs were classified as cardiomyocyte-enriched, noncardiomyocyte-enriched or nonenriched at an enrichment ratio ≥2, ≤0.5 or 0.5-2.0, respectively (**Expanded Methods**). mRNA fold-change and FDR (<0.02) are shown for each of 1 and 2 wk TAC vs sham.

**Supplemental Table 4** is supplied as an Excel (.xls) file.

**Supplemental Table 5.** Cardiomyocyte and nonmyocyte distribution of TAC-regulated microRNAs. MicroRNAs were classified cardiomyocyte-enriched, noncardiomyocyte-enriched or nonenriched at an enrichment ratio ≥2, ≤0.5 or 0.5-2.0, respectively (**Expanded Methods**). MicroRNA fold-change and FDR (<0.02) are shown for 1 wk TAC and are reprocessed from NCBI GEO GSE56891 [8].

**Supplemental Table 5** is supplied as an Excel (.xls) file.

**Supplemental Table 6. A)** Direct mRNA targets of miR-133a under unstressed conditions. Direct mRNA targets of the miR-133a transgene in unstressed hearts, identified using RISC-seq procedures (**Expanded Methods**), are listed (FDR<0.02). Cardiomyocyte enrichment ratios for individual mRNAs are calculated as described in **Expanded Methods**. fc, fold-change; FDR, false-discovery rate; FPKM, fragments per kb of exon per million mapped (aligned) reads. TargetScan 6.2 predictions [26] were taken from the 2012 mouse conserved and nonconserved site database; an entry in this column denotes the type of miR-mRNA site match. miRDB predictions

[27] were obtained from the 2014 database release; entries in this column denote the mRNA RefSeq transcript predicted to bind to miR-133a. **B)** mRNAs indirectly regulated by miR-133a overexpression under unstressed conditions. As for **A)** but without TargetScan or miRDB annotations; category designations are NU = no RISC change, global RNA up; ND = no RISC change, global mRNA down. **C)** 'Tracking' set of direct miR-133a targets and fate in response to TAC. **D**) 'Tracking' set of indirect miR-133a targets and fate in response to TAC.

**Supplemental Table 6** is supplied as an Excel (.xls) file.

**Supplemental Table 7. A)** Direct mRNA targets of miR-378 under unstressed conditions. Direct mRNA targets of the miR-378 transgene in unstressed hearts, identified using RISC-seq procedures (**Supplemental Methods**), are listed (FDR<0.02). Cardiomyocyte enrichment ratios for individual mRNAs are calculated as described in **Expanded Methods**. fc, fold-change; FDR, false-discovery rate; FPKM, fragments per kb of exon per million mapped (aligned) reads. TargetScan 6.2 predictions [26] were taken from the 2012 mouse conserved and nonconserved site database; an entry in this column denotes the type of miR-mRNA site match. miRDB predictions [27] were obtained from the 2014 database release; however no matches were found between transcripts predicted to bind to miR-378 and empirical data. **B)** mRNAs indirectly regulated by miR-378 overexpression under unstressed conditions. As for **A)** but without TargetScan or miRDB annotations; category designations are NU = no RISC change, global RNA up; ND = no RISC change, global mRNA down. **C)** 'Tracking' set of direct miR-378 targets and fate in response to TAC. **D**) 'Tracking' set of indirect miR-378 targets and fate in response to TAC.

**Supplemental Table 7** is supplied as an Excel (.xls) file.

**Supplemental Table 8.** RISC-derepression of mRNAs in response to microRNA overexpression in cardiomyocytes. mRNAs whose abundance in the RISC fraction decreased, with converse change or no change in the global mRNA fraction (FDR<0.02), in response to the αMHC-miR-133a transgene (**A**) or the αMHC-miR-378 transgene (**B**).

**Supplemental Table 8** is supplied as an Excel (.xls) file.

**Additional References**


1. Gulick J, Subramaniam A, Neumann J, Robbins J. Isolation and characterization of the mouse cardiac myosin heavy chain genes. *J Biol Chem.* 1991;266:9180-9185.
2. Matkovich SJ, Wang W, Tu Y, Eschenbacher WH, Dorn LE, Condorelli G, et al. MicroRNA-133a protects against myocardial fibrosis and modulates electrical repolarization without affecting hypertrophy in pressure-overloaded adult hearts. *Circ Res.* 2010;106:166-175.
3. Matkovich SJ, Hu Y, Dorn GW, 2nd. Regulation of cardiac microRNAs by cardiac microRNAs. *Circ Res.* 2013;113:62-71.
4. Dorn GW, 2nd, Robbins J, Ball N, Walsh RA. Myosin heavy chain regulation and myocyte contractile depression after LV hypertrophy in aortic-banded mice. *Am J Physiol Heart Circ Physiol.* 1994;267:H400-405.
5. Souders CA, Borg TK, Banerjee I, Baudino TA. Pressure overload induces early morphological changes in the heart. *Am J Pathol.* 2012;181:1226-1235.
6. Griffiths-Jones S, Grocock RJ, van Dongen S, Bateman A, Enright AJ. miRBase: microRNA sequences, targets and gene nomenclature. *Nucleic Acids Res.* 2006;34:D140-144.
7. Kozomara A, Griffiths-Jones S. miRBase: integrating microRNA annotation and deep-sequencing data. *Nucleic Acids Res.* 2011;39:D152-157.
8. Hu Y, Matkovich SJ, Hecker PA, Zhang Y, Dorn GW, II. Epitranscriptional orchestration of genetic reprogramming is an emergent property of stress-regulated cardiac microRNAs. *Proc Natl Acad Sci USA.* 2012;109:19864-19869.
9. Hackenberg M, Rodriguez-Ezpeleta N, Aransay AM. miRanalyzer: an update on the detection and analysis of microRNAs in high-throughput sequencing experiments. *Nucleic Acids Res.* 2011;39:W132-138.
10. Matkovich SJ, Hu Y, Eschenbacher WH, Dorn LE, Dorn GW, II. Direct and indirect involvement of microRNA-499 in clinical and experimental cardiomyopathy. *Circ Res.* 2012;111:521-531.
11. Dorn GW, 2nd, Matkovich SJ, Eschenbacher WH, Zhang Y. A human 3' miR-499 mutation alters cardiac mRNA targeting and function. *Circ Res.* 2012;110:958-967.
12. Matkovich SJ, Van Booven DJ, Eschenbacher WH, Dorn GW, 2nd. RISC RNA sequencing for context-specific identification of in vivo microRNA targets. *Circ Res.* 2011;108:18-26.
13. Matkovich SJ, Zhang Y, Van Booven D, Dorn GW, 2nd. Deep mRNA sequencing for in vivo functional analysis of cardiac transcriptional regulators. Application to Gαq. *Circ Res.* 2010;106:1459-1467.
14. Trapnell C, Roberts A, Goff L, Pertea G, Kim D, Kelley DR, et al. Differential gene and transcript expression analysis of RNA-seq experiments with TopHat and Cufflinks. *Nat Protoc.* 2012;7:562-578.
15. Trapnell C, Pachter L, Salzberg SL. TopHat: discovering splice junctions with RNA-Seq. *Bioinformatics.* 2009;25:1105-1111.
16. Anders S, Huber W. Differential expression analysis for sequence count data. *Genome Biol.* 2010;11:R106.

17. Martin HC, Wani S, Steptoe AL, Krishnan K, Nones K, Nourbakhsh E, et al. Imperfect centered miRNA binding sites are common and can mediate repression of target mRNAs. *Genome Biol.* 2014;15:R51.
18. Hausser J, Syed AP, Bilen B, Zavolan M. Analysis of CDS-located miRNA target sites suggests that they can effectively inhibit translation. *Genome Res.* 2013;23:604-615.
19. Liu Q, Halvey PJ, Shyr Y, Slebos RJ, Liebler DC, Zhang B. Integrative omics analysis reveals the importance and scope of translational repression in microRNA-mediated regulation. *Mol Cell Proteomics.* 2013;12:1900-1911.
20. Horman SR, Janas MM, Litterst C, Wang B, MacRae IJ, Sever MJ, et al. Akt-mediated phosphorylation of Argonaute 2 downregulates cleavage and upregulates translational repression of microRNA targets. *Mol Cell.* 2013;50:356-367.
21. Huntzinger E, Izaurralde E. Gene silencing by microRNAs: contributions of translational repression and mRNA decay. *Nat Rev Genet.* 2011;12:99-110.
22. Thomson_Reuters. MetaCore. Available at: http://www.genego.com. Accessed 4/2/14.
23. Huang DW, Sherman BT, Lempicki RA. Systematic and integrative analysis of large gene lists using DAVID bioinformatics resources. *Nat Protoc.* 2009;4:44-57.
24. Janes KA. An analysis of critical factors for quantitative immunoblotting. *Sci Signal.* 2015;8:rs2.
25. Nagalingam RS, Sundaresan NR, Gupta MP, Geenen DL, Solaro RJ, Gupta M. A cardiac-enriched microRNA, miR-378, blocks cardiac hypertrophy by targeting Ras signaling. *J Biol Chem.* 2013;288:11216-11232.
26. Garcia DM, Baek D, Shin C, Bell GW, Grimson A, Bartel DP. Weak seed-pairing stability and high target-site abundance decrease the proficiency of lsy-6 and other microRNAs. *Nat Struct Mol Biol.* 2011;18:1139-1146.
27. Wang X, El Naqa IM. Prediction of both conserved and nonconserved microRNA targets in animals. *Bioinformatics.* 2008;24:325-332.